



Bound states in the continuum (BIC) in silicon nanodisk array on mirror structure: Perfect absorption associated with quasi-BIC below the bandgap

Moriasa, Keisuke
Hasebe, Hiroaki
Sugimoto, Hiroshi
Fujii, Minoru

(Citation)

Journal of Applied Physics, 133(17):173102

(Issue Date)

2023-05-07

(Resource Type)

journal article

(Version)

Version of Record

(Rights)

© 2023 Author(s). Published under an exclusive license by AIP Publishing.
This article may be downloaded for personal use only. Any other use requires prior permission of the author and AIP Publishing. This article appeared in Journal of Applied Physics 133, 173102 (2023) and may be found at...


(URL)

<https://hdl.handle.net/20.500.14094/0100482763>



RESEARCH ARTICLE | MAY 01 2023

Bound states in the continuum (BIC) in silicon nanodisk array on mirror structure: Perfect absorption associated with quasi-BIC below the bandgap

Keisuke Moriasa; Hiroaki Hasebe; Hiroshi Sugimoto ; ... et. al



Journal of Applied Physics 133, 173102 (2023)

<https://doi.org/10.1063/5.0146896>



View Online



Export Citation

CrossMark



Time to get excited.
Lock-in Amplifiers – from DC to 8.5 GHz

[Find out more](#)

Bound states in the continuum (BIC) in silicon nanodisk array on mirror structure: Perfect absorption associated with quasi-BIC below the bandgap

Cite as: J. Appl. Phys. **133**, 173102 (2023); doi: [10.1063/5.0146896](https://doi.org/10.1063/5.0146896)

Submitted: 17 February 2023 · Accepted: 11 March 2023 ·

Published Online: 1 May 2023



View Online



Export Citation



CrossMark

Keisuke Moriasa, Hiroaki Hasebe, Hiroshi Sugimoto, ^{a)} and Minoru Fujii ^{a)}

AFFILIATIONS

Department of Electrical and Electronic Engineering, Graduate School of Engineering, Kobe University, Rokkodai, Nada, Kobe 657-8501, Japan

^{a)}Authors to whom correspondence should be addressed: sugimoto@eedept.kobe-u.ac.jp and fujii@eedept.kobe-u.ac.jp

ABSTRACT

A structure composed of a hexagonal array of Si nanodisks having toroidal dipole resonances and a reflecting mirror separated by a SiO₂ spacer is proposed as a platform that exhibits narrow-band perfect absorption in the Si sub-bandgap wavelength range for a CMOS compatible Si based photodetector operating below the bandgap range. The numerical simulation reveals that the structure possesses Fabry-Pérot bound states in the continuum at proper spacer thicknesses due to the interference between the toroidal dipole and its image dipole. By slightly detuning the spacer thickness to meet the critical coupling condition, narrow-band perfect absorption appears despite assumption of a very small extinction coefficient (5×10^{-4}). The wavelength of the perfect absorption is controlled in a wide range by the structural parameters of a Si nanodisk hexagonal array and is insensitive to the fluctuation of the extinction coefficient and the choice of a metallic mirror. In the structure, over 90% of incident power can be absorbed in the Si region. This suggests that the structure can be used as a narrow-band photodetector operating in the Si sub-bandgap wavelength range. We also evaluate the sensing performance of the proposed structure as an intensity based refractive index sensor operating in the near-infrared range.

Published under an exclusive license by AIP Publishing. <https://doi.org/10.1063/5.0146896>

I. INTRODUCTION

Near-infrared light beyond 1400 nm has high eye safety because it is strongly absorbed in the outer layer of the eye, such as cornea, vitreous, and lens, and cannot reach more sensitive retina.^{1,2} Since conventional silicon (Si) photodetectors are transparent in this range, narrow-bandgap semiconductors, such as InGaAs, SiGe, and Ge, are usually used as a monolithic device or are integrated in Si-based devices.³ Recently, a new concept that uses near-infrared absorption by localized surface plasmon resonances of noble metal nanostructures and hot electron injection at a metal/Si Schottky junction has been proposed as a new Si-based photodetector operating below the bandgap,^{4,5} and the performance of this type of device has been improving rapidly.⁶⁻⁹ A drawback of the device is the requirement of a noble metal that is not compatible with conventional CMOS processes.

Another approach to detect below-bandgap photons is utilizing defect-mediated light absorption.¹⁰⁻¹³ Since defect-mediated sub-bandgap absorption of Si is very weak, i.e., the extinction coefficient (κ) is $\sim 10^{-3}$ or less,^{11,13} absorption enhancement by optical resonances is crucial for the practical usage. For example, narrow-band photodetection around 1500 nm is achieved by using Mie resonances (whispering gallery mode) of a micron-meter size Si sphere.¹² In our previous work, we used toroidal dipole (TD) resonances supported by a hexagonal array of Si nanodisks for the sub-bandgap absorption enhancement. The TD mode destructively interferes with the Cartesian electric dipole (ED) mode and forms a nonradiating anapole state, which enhances light absorption,^{14,15} photocatalytic activity,¹⁶ and nonlinear optical effects.^{17,18} We experimentally demonstrated narrow-band photocurrent enhancement around 1550 nm by the TD resonances in a Si nanodisk

hexagonal array.¹⁴ An advantage of this approach, i.e., enhancement of defect-mediated sub-bandgap absorption by optical resonances to detect sub-bandgap photons, is the unnecessary of noble metals and a simple structure. A drawback is the inefficient photon-to-electron conversion efficiency that arises from the fact that several photons are required to excite an electron to the conduction band. Therefore, to make this type of device practically useful, very strong absorption enhancement is necessary.

Absorptance of a system consisting of an optical resonator supporting a single resonant mode is described by the temporal coupled mode theory (TCMT) as^{19–21}

$$A = \frac{4}{m} \frac{\gamma\delta}{(\omega - \omega_0)^2 + (\gamma + \delta)^2}, \quad (1)$$

where m is the number of free-space ports in the system, ω_0 is the resonant frequency, and γ and δ are radiation and absorption loss rates, respectively. The absorptance becomes maximum at the critical coupling condition where the radiation and absorption losses are equal ($\gamma = \delta$). If a metasurface supports a single resonant mode and has two radiating ports ($m = 2$), the theoretical limit of the absorptance is 50%. To overcome this theoretical limit, several strategies have been proposed. One of them is using two degenerate resonant modes with opposite symmetry (degenerate critical coupling).^{20,22–25} For example, perfect absorption ($A = 1$) is achieved in Si metasurfaces with degenerate electric dipole (ED) and magnetic dipole (MD) modes.^{23,24} Another approach is introducing a reflecting mirror below a resonator to suppress the transmission, i.e., to close one of the radiating ports ($m = 1$).²² In both approaches, an important aspect to achieve perfect absorption is precise tuning of the balance between the radiation and absorption losses. In order to achieve the critical coupling condition in a low-loss sub-bandgap range, the radiation loss of a resonator should be very small.

Precise control of a radiation loss of a resonator can be achieved by using optical bound states in the continuum (BICs). BIC is an electromagnetic state with zero radiation loss located inside the light cone.^{26,27} Although BIC has infinite quality factors and cannot be coupled from the far-field, a slight deviation from a BIC condition results in so-called quasi-BIC, which has a finite quality factor (radiation loss). The quasi-BIC has been used for the enhancement of light absorption,²⁴ nonlinear optical effects,^{28–30} photocatalytic activity,³¹ bio-sensing,^{32,33} and lasers.^{34,35}

In this work, we combine TD resonances of a Si nanodisk hexagonal array and BIC and propose a structure having narrow-band perfect absorption (PA) below the bandgap. The proposed structure is composed of a Si nanodisk hexagonal array and a reflecting mirror separated by a SiO₂ spacer of hundreds of nanometers to 1 μm in thickness. We demonstrate from numerical simulations that the structure has Fabry-Pérot BIC (FP-BIC) at proper nanodisk-mirror distances.^{26,28,36,37} By detuning the distance from the BIC conditions, the radiation loss can be tuned to match the material loss, and it results in narrow-band perfect absorption. We show that more than 90% of incident power can be absorbed by a Si at the critical coupling conditions. Finally, we investigate the potential of the structure as a photocurrent detection type refractive index sensing device.

II. RESULTS AND DISCUSSION

Figure 1(a) shows the schematic illustration of a Si nanodisk hexagonal array formed on a Si thin film,^{14,38} and Fig. 1(b) shows the calculated transmittance (T), reflectance (R), and absorptance ($A = 1 - T - R$) spectra under normal incidence. The structural parameters [diameter (D) and height (h) of a nanodisk, array pitch (P), and Si film thickness (t)] are shown in Fig. 1(a). For the calculations, we fixed the refractive index of Si (n) to 3.5 because of the small dispersion below the bandgap. The extinction coefficient (κ) is assumed to be 5×10^{-4} , which is the smallest value reported for poly-Si around 1500 nm.^{10,11} Despite the very small extinction coefficient, a clear absorption peak appears at 1571.4 nm. The electric field distributions ($|E|/|E_0|$) in the xy ($z = h/2$) and yz ($x = 0$) planes at the peak wavelength are shown in Fig. 1(c). We can see the symmetric current loops characteristic of the TD resonance in the xy plane.^{14,29,39} The electric field is tightly confined in the Si nanodisk region, and the confinement leads to strong absorption enhancement. In this structure, the maximum absorptance is $\sim 3\%$. This value can be increased by optimizing the structural parameters^{14,38} but cannot exceed 50% because of the existence of the two radiating ports ($m = 2$) [Fig. 1(a)].

To overcome this limitation, we propose a structure that has a mirror below the nanodisk array as schematically shown in Fig. 2(a). The mirror closes the radiating port 2, and thus, the maximum absorptance can reach unity. This structure can be modeled by the image dipole method [Fig. 2(b)],^{18,40} in which the mirror works as a mirror dipole for a toroidal dipole in a Si nanodisk. The structure in Fig. 2(a) is, thus, regarded as two resonators separated by twice the spacer thickness (S), and their interference determines the optical response. Figure 2(c) shows a schematic illustration of a near- and far-field coupled resonator system, ζ is the near-field coupling constant, and ψ is the propagating phase shift between the two resonators. In the absence of an external driving source, the oscillation amplitudes of the two resonators (a_1, a_2) are described by the TCMT as³⁶

$$\frac{d}{dt} \begin{pmatrix} a_1 \\ a_2 \end{pmatrix} = \left[i \begin{pmatrix} \omega_0 & \zeta \\ \zeta & \omega_0 \end{pmatrix} - \gamma_0 \begin{pmatrix} 1 & e^{-i\psi} \\ e^{-i\psi} & 1 \end{pmatrix} \right] \begin{pmatrix} a_1 \\ a_2 \end{pmatrix}. \quad (2)$$

In a time harmonic field ($a_k = A_k e^{i\omega t}$) and a steady-state, Eq. (2) becomes

$$\begin{bmatrix} i(\omega - \omega_0) - \gamma_0 & i\zeta - \gamma_0 e^{-i\psi} \\ i\zeta - \gamma_0 e^{-i\psi} & i(\omega - \omega_0) - \gamma_0 \end{bmatrix} \begin{pmatrix} A_1 \\ A_2 \end{pmatrix} = \begin{pmatrix} 0 \\ 0 \end{pmatrix}. \quad (3)$$

The eigenvalues and eigenvectors are, thus,

$$\omega_{\pm} = \omega_0 \pm (\zeta + \gamma_0 \sin\psi) + i\gamma_0(1 \pm \cos\psi) \quad (4)$$

and

$$\begin{pmatrix} A_1 \\ A_2 \end{pmatrix} = \begin{pmatrix} 1 \\ \pm 1 \end{pmatrix}, \quad (5)$$

respectively. When the phase shift ψ is equal to an integer multiple of 2π , the imaginary part disappears at ω_{\pm} and the mode cannot

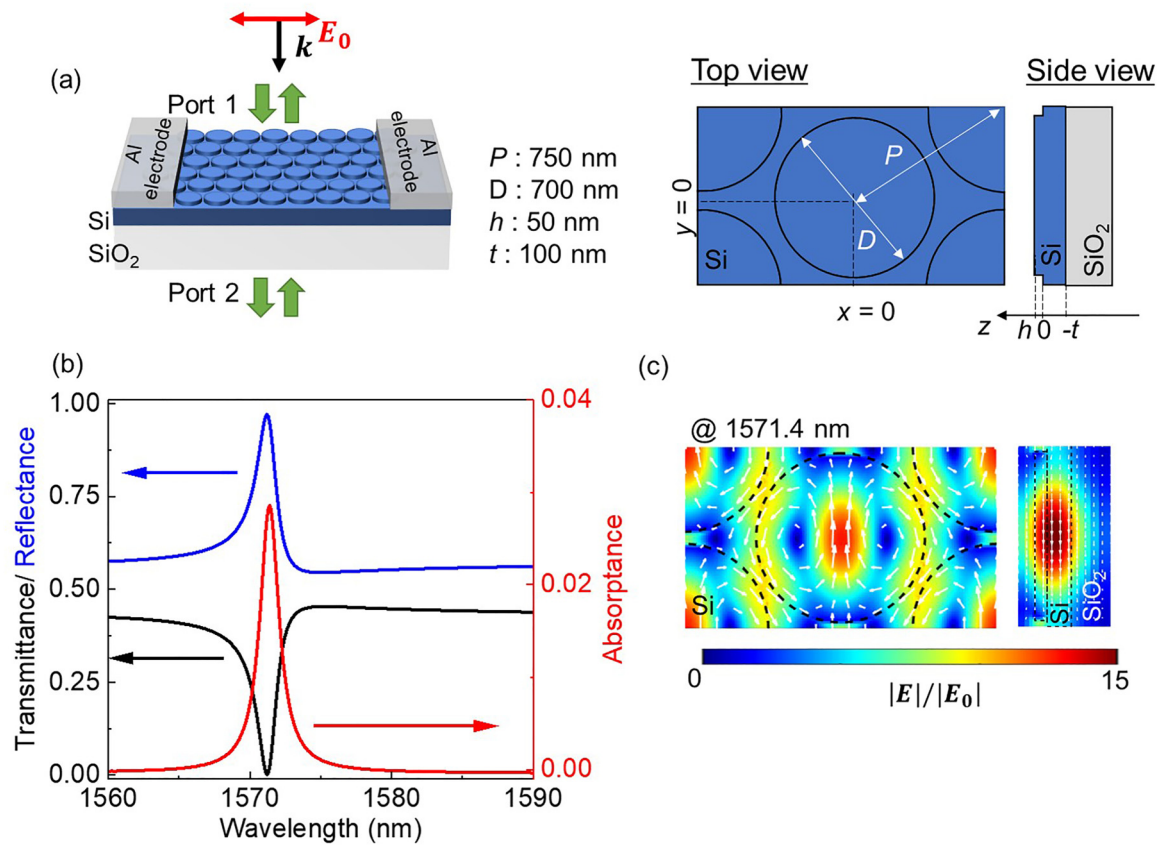


FIG. 1. (a) (left) Schematic illustration of a Si nanodisk hexagonal array formed on a Si thin film. The wavevector (k) of incident light is normal to the surface. (Right) Top and side views of the structure and definition of the structural parameters. (b) Calculated transmittance (black), reflectance (blue), and absorbance (red) spectra of a Si nanodisk hexagonal array with $P = 750 \text{ nm}$, $D = 700 \text{ nm}$, $h = 50 \text{ nm}$, and $t = 100 \text{ nm}$. (c) Electric field distributions ($|E|/|E_0|$) in xy ($z = h/2$) and yz ($x = 0$) planes at 1571.4 nm . Electric field vectors are also shown by white arrows.

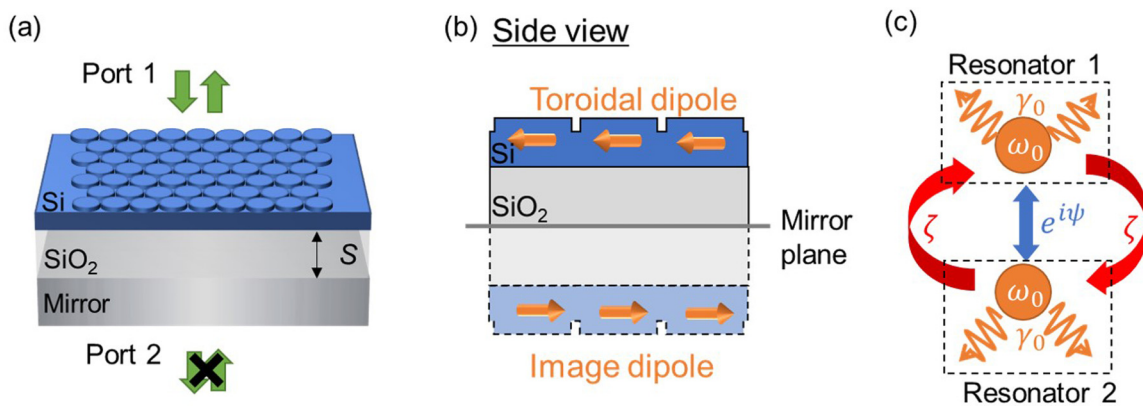


FIG. 2. (a) Schematic illustration of a silicon nanodisk hexagonal array on a mirror structure. (b) Image dipole model to calculate the optical response of the structure in (a) when TD resonance is excited in a Si nanodisk. (c) Schematic illustration of near and far-field coupling of two resonators. ω_0 and γ_0 are the resonant frequency and the radiation loss rate of individual resonators. ζ and ψ are the near-field coupling strength and the propagating phase shift, respectively.

Downloaded from http://pubs.aip.org/jap/article-pdf/doi/10.1063/5.0146896/17230497/173102_1_5.0146896.pdf

exchange energy with free space. This is the FP-BICs.^{26,36} In the structure in Fig. 2(a), the phase shift can be tuned by the spacer thickness (S). Detuning the phase shift from the FP-BIC conditions allows us to control the degree of the energy exchange with free

space, i.e., the radiation loss rate γ , to meet the material loss δ to realize perfect absorption.

We now calculate the absorptance spectra of the structure in Fig. 2(a) by systematically changing the phase shift ψ by the spacer

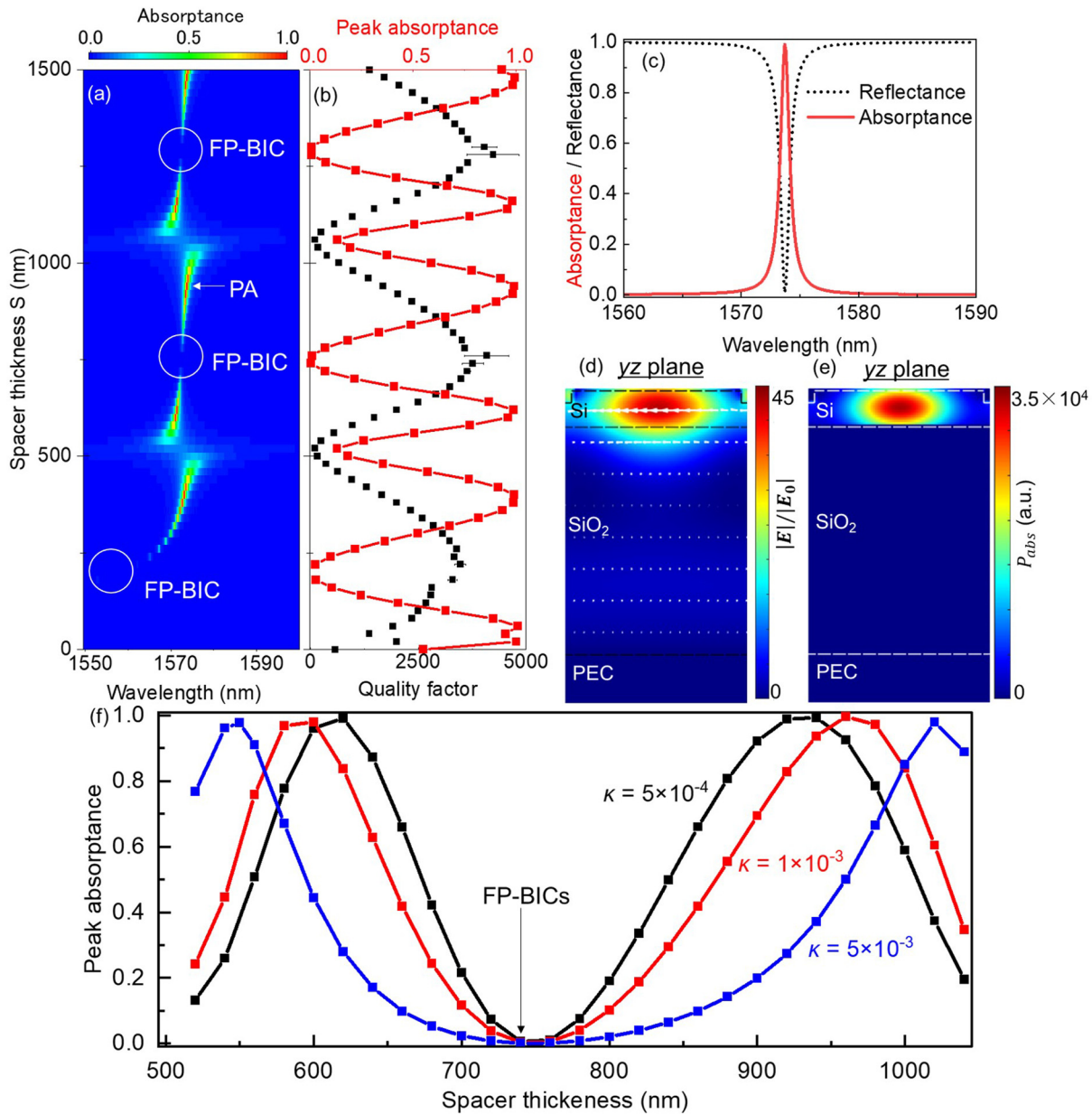


FIG. 3. (a) Contour plot of absorptance as functions of wavelength and spacer thickness. Other structural parameters are $P=750$ nm, $D=700$ nm, $h=50$ nm, and $t=100$ nm. (b) Quality factor (black) and peak absorptance (red) as a function of spacer thickness (vertical axis) at the TD resonance around 1570 nm. (c) Reflectance (broken black curve) and absorptance (solid red curve) spectra when the spacer thickness is 940 nm [indicated by a white arrow in Fig. 2(a)]. (d) and (e) Electric field (d) and absorbed power (e) distributions in the yz ($x=0$) plane at 1573.7 nm. (f) Peak absorptance as a function of spacer thickness calculated for different values of extinction coefficient ($\kappa = 5 \times 10^{-4}$, 1×10^{-3} , and 5×10^{-3}) and a fixed refractive index ($n = 3.5$).

Downloaded from http://pubs.aip.org/jap/article-pdf/doi/10.1063/5.0146896/17230497/173102_1_5.0146896.pdf

thickness S . First, we assume a lossless perfect electric conductor (PEC) as a mirror and later consider a real material, such as aluminum (Al) and gold (Au). Figure 3(a) shows the contour plot of the absorptance as functions of the wavelength and the spacer thickness. Other structural parameters are the same as those in Fig. 1(a). The incident light is normal to the surface. We can see an absorption peak around 1570 nm due to the TD resonance for $S \geq 250$, while for $S \leq 250$ nm, the near-field coupling shifts the resonance to a shorter wavelength (see Fig. S1 in the supplementary material). The absorptance is periodically modified by S , and at $S = 200, 760$, and 1280 nm, it is very close to zero. This is the FP-BIC; i.e., the resonators cannot exchange energy with free space and the incident light is nearly 100% reflected ($R \approx 1$). In Fig. 3(b), the quality factor obtained by fitting the absorption peaks with a Lorentz function is plotted as a function of spacer thickness. It takes the maximum value of 3500–4000 at the BIC conditions. This value is close to that estimated from the material loss ($n/2\kappa = 3500$) for $n = 3.5$ and $\kappa = 5 \times 10^{-4}$.⁴¹

If we detune (e.g., increase) the spacer thickness from the FP-BIC conditions, the radiation loss rate γ has a finite value, and if γ reaches the critical coupling condition ($\delta = \gamma$), the absorptance becomes the maximum. A further increase of the spacer thickness results in the overcoupling condition ($\delta < \gamma$) and the absorptance decreases. In Fig. 3(b), the value of the peak absorptance is plotted as a function of the spacer thickness. At the critical coupling condition ($S = 20, 60, 400, 620, 940, 1160$, and 1480 nm), the peak absorptance reaches nearly unity. Figure 3(c) shows the reflectance and absorptance spectra at $S = 940$ nm. The absorptance is over 0.99 at the resonance, and the Q factor is 1692. Figures 3(d) and 3(e) shows the electric field and the absorbed power distribution in the yz -plane, respectively. The electric field is concentrated on the Si region and the maximum enhancement factor reaches >40 , which is threefold larger than that of the structure without the mirror [Fig. 1(c)].

Up to now, we assume the extinction coefficient of Si to be 5×10^{-4} . Since the extinction coefficient of poly-Si depends on the deposition methods and conditions,^{10,11} we investigate the effect of the excitation coefficient value on the absorption property. In Fig. S2 of the supplementary material, we show the data similar to Fig. 3(a) obtained for $\kappa = 5 \times 10^{-4}$, 1×10^{-3} , and 5×10^{-3} . The data indicate that the extinction coefficient does not strongly affect the BIC condition ($S \approx 760$ nm), while the condition of the perfect absorption depends on the extinction coefficient. Figure 3(f) shows the peak absorptance as a function of the spacer thickness for three different values of the extinction coefficient. We can see that materials with larger losses require a larger deviation from the BIC condition to satisfy the critical coupling condition. By properly controlling the spacer thickness, perfect absorption is achieved in the wide extinction coefficient range ($\kappa = 5 \times 10^{-4} - 5 \times 10^{-3}$). Note that the resonance wavelength is very insensitive to the extinction coefficient (see Fig. S2 in the supplementary material), and thus, a small fluctuation of the extinction coefficient from a designed value does not strongly affect the resonance wavelength, although it slightly decreases the absorptance value.

The resonance wavelength of the proposed structure can be controlled by the structural parameters of the nanodisk array. Figure 4(a) shows contour plots of absorptance as functions of the wavelength and the spacer thickness when the thickness of a Si

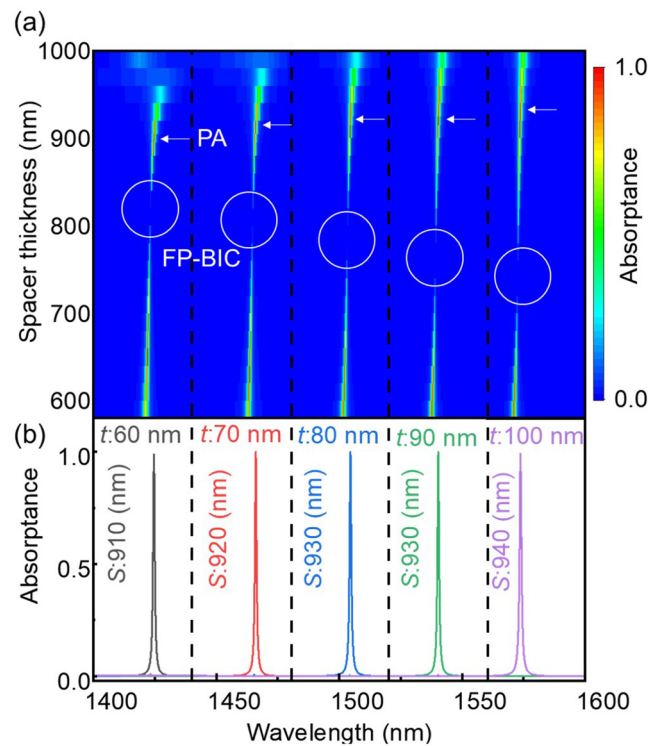


FIG. 4. (a) Contour plots of absorptance as functions of wavelength and spacer thickness. From left to right, the Si thin film thickness (t) is increased from 60 to 100 nm. Other structural parameters are $P = 750$ nm, $D = 700$ nm, and $h = 50$ nm. (b) Absorption spectra at the critical coupling conditions indicated by white arrows in Fig. 4(a).

film below a nanodisk array (t) is changed from 60 to 100 nm. The TD resonance wavelength changes from ~ 1420 to ~ 1570 nm for $t = 60$ –100 nm. This shift is due to increased confinement volume of the electric field. In Fig. 4(a), the BIC and perfect absorption conditions are shown by circles and arrows, respectively. The optimum spacer thickness for BIC decreases with increasing t . Figure 4(b) shows the absorption spectra at the spacer thicknesses designated by arrows in Fig. 4(a). Narrow-band perfect absorption is achieved in the 1420–1570 nm range. It is worth noting that the absorption spectra are independent of the polarization direction of incident light due to the C_6 symmetry of the structure (Fig. S3 in the supplementary material).

We now replace the PEC mirror with an Al one. Figure 5(a) shows a contour plot of the absorptance as functions of the wavelength and the spacer thickness calculated assuming an Al mirror. The resonance wavelength of the TD mode is around 1570 nm, which is very close to the case of the PEC mirror [Fig. 3(a)]. Furthermore, BIC appears at almost the same spacer thicknesses, e.g., $S = 180, 750$, and 1280 nm. One of the differences between a PEC and an Al mirror is the spectral shape when the wavelengths of the Fabry-Pérot interferences and the TD resonances are overlapped ($S \approx 500$ and 1040 nm). In an Al mirror, the peak has a

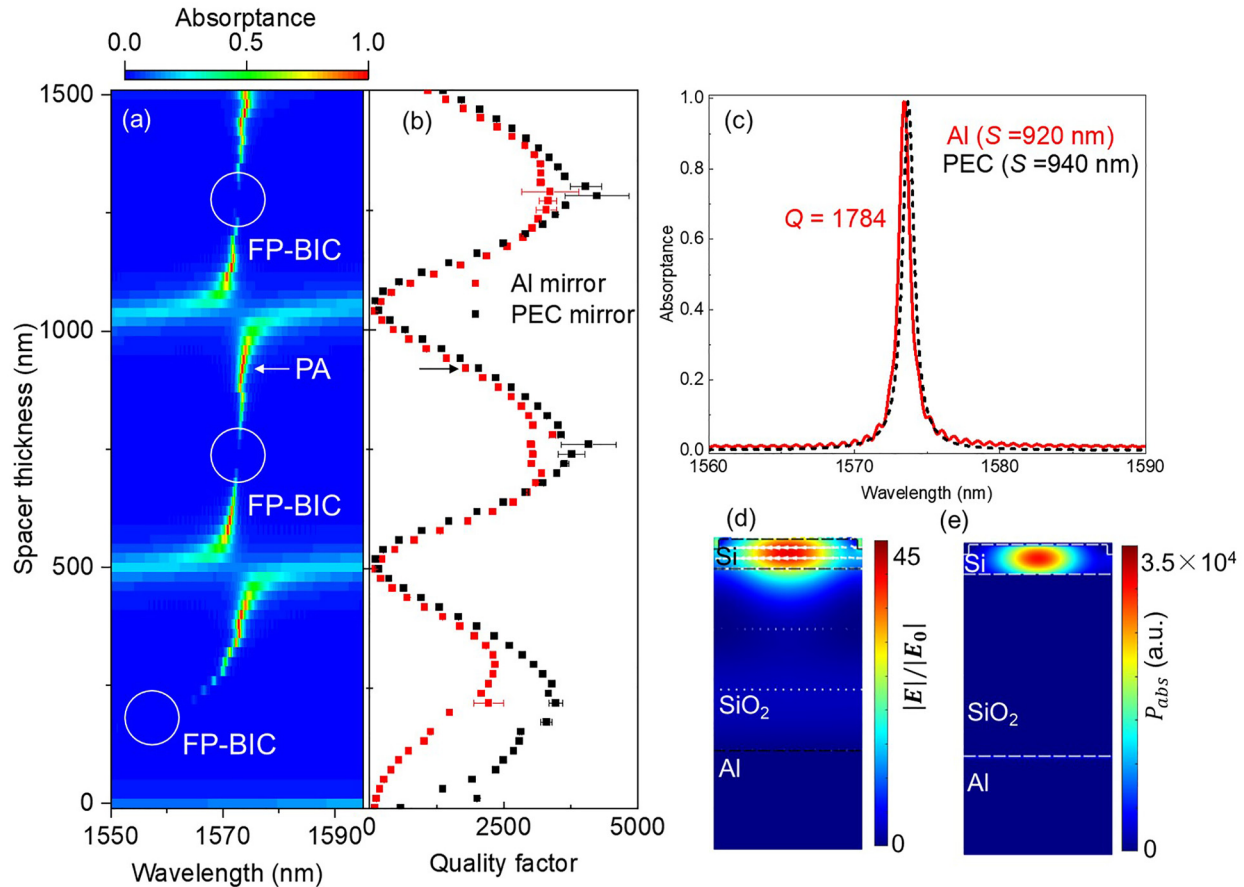


FIG. 5. (a) Contour plot of absorptance as functions of wavelength and spacer thickness for a Si nanodisk hexagonal array on an Al mirror structure. Other structural parameters are $P=750$ nm, $D=700$ nm, $h=50$ nm, and $t=100$. (b) Quality factor of an absorptance peak as a function of spacer thickness calculated from the data in (a) (red). The quality factor calculated for a PEC mirror is also shown (black). (c) Calculated absorptance spectra for an Al mirror (red solid curve) ($S=920$ nm) and for a PEC mirror (black broken curve) ($S=940$ nm). (d) Electric field and (e) absorbed power distributions in the yz ($x=0$) plane at 1573.4 nm.

Fano-type highly asymmetric shape (see Fig. S4 in the [supplementary material](#)), while in a PEC mirror, it is well-fitted by the Lorentzian function. We fitted the asymmetric peak with a generalized Fano function⁴² to extract the quality factor. Figure 5(b) shows the quality factor of the absorption peak as a function of the spacer thickness. The quality factor decreases slightly by replacing a PEC mirror with an Al mirror at the BIC conditions, while the difference is very small at the perfect absorption conditions. The degradation of the quality factor is due to absorption by an Al mirror (Fig. S5 in the [supplementary material](#)). Figure 5(c) compares the absorptance spectra at the critical coupling conditions between a PEC mirror ($S=940$ nm) and an Al mirror ($S=920$ nm). High quality factor perfect absorption is achieved by using a lossy Al mirror. Figures 5(d) and 5(e) show the electric field and absorbed power distributions at the peak wavelength in Fig. 5(c). The electric field is tightly confined in the Si region. 93% of incident power is absorbed in the Si region, and 7% is absorbed by the Al mirror.

Therefore, large photocurrent enhancement is expected in a Si nanodisk array with an Al mirror. Similar results are obtained when we use an Au mirror (Fig. S6 in the [supplementary material](#)). On the other hand, if we use a crystalline Si mirror, perfect absorption cannot be achieved due to the leakage of the field to the bottom (Fig. S6 in the [supplementary material](#)).

A possible application of the narrow-band photodetection by a Si nanodisk array on a mirror structure is a spectrometer-free, current-detection-type refractive index sensor operating in the second near-infrared biological window.^{43–46} The capability to detect the absorption peak shift directly as a photocurrent change makes the device much simpler than that using an external photodetector and a spectrometer.⁴⁷ To estimate the sensitivity, we calculate the absorptance for different background refractive indices ($n=1.30$ – 1.40) [Fig. 6(a)]. The absorption peak redshifts with increasing the refractive index, while the absorptance is kept at ~ 1 . Figure 6(b) shows the peak wavelength and the absorptance

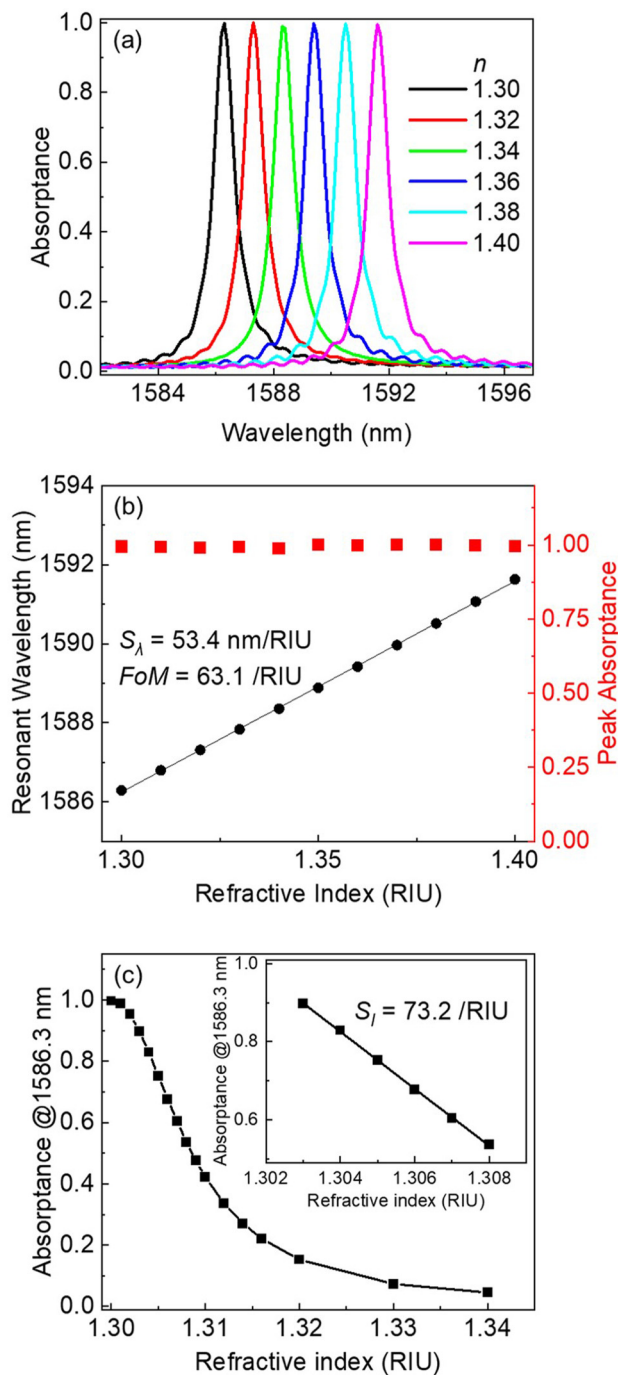


FIG. 6. (a) Calculated absorbance spectra of a Si nanodisk array on an Al mirror structure with different surrounding medium ($n = 1.3\text{--}1.4$). The structural parameters are $P = 750 \text{ nm}$, $D = 700 \text{ nm}$, $h = 50 \text{ nm}$, $t = 100 \text{ nm}$, and $S = 920 \text{ nm}$. (b) Resonant wavelength and peak absorbance as a function of the refractive index of the surrounding medium. (c) Absorbance as a function of the refractive index of the surrounding medium at the resonant wavelength (1586.3 nm).

as a function of the refractive index. The sensitivity $S_\lambda = \Delta\lambda/\Delta n$ estimated from Fig. 6(b) is 53.4 nm/RIU, and the figure of merit defined by the sensitivity divided by the full width at half maximum (FWHM) of the peak ($FoM = S/\text{FWHM}$) is 63.1/RIU. Figure 6(c) shows the absorbance at 1586.3 nm (peak wavelength for $n = 1.3$) as a function of the refractive index of an environment. Because of the narrow absorption band and the large range of the absorbance change, the value is very sensitive to the refractive index change. The intensity refractive index sensitivity defined by $S_I = \Delta A/\Delta n$ ^{48,49} is 73.2/RIU in the range of $n = 1.303\text{--}1.308$.

III. CONCLUSION

We design a structure composed of a Si nanodisk hexagonal array having TD resonances and a mirror separated by a SiO_2 spacer. The structure has FP-BICs arising from the interference between a TD and a mirror dipole. We show that by detuning the BIC conditions by controlling the spacer thickness, the critical coupling condition is achieved and narrow-band perfect absorption appears in the region where the extinction coefficient of Si is very small. The wavelength of the perfect absorption is controlled by the structural parameters of a Si nanodisk hexagonal array and is insensitive to the variation of the extinction coefficient and the choice of a metallic mirror. In the structure, over 90% of incident power can be absorbed in the Si region. This suggests that this structure can be used as a narrow-band photodetector operating in the Si sub-bandgap wavelength range.

SUPPLEMENTARY MATERIAL

See the [supplementary material](#) for the details on the numerical simulation method, absorbance spectra of a Si nanodisk array on PEC in the thin spacer thickness range, absorbance spectra of a Si nanodisk array on PEC with a different extinction coefficient of Si, absorbance spectra of a Si nanodisk array on PEC under different polarization of incident light, fitting of an absorption spectrum with a generalized Fano function, an electric field and an absorbed power distribution of a Si nanodisk array on Al without the spacer, and absorbance spectra of a Si nanodisk array on Au and Si mirrors.

ACKNOWLEDGMENTS

This work was partially supported by the JSPS KAKENHI (Grant Nos. 18KK0141, 21H01748, 21H01782, 21K14496, and 22K18949).

AUTHOR DECLARATIONS

Conflict of Interest

The authors have no conflicts to disclose.

Author Contributions

Keisuke Moriasa: Conceptualization (equal); Data curation (equal); Methodology (equal); Writing – original draft (equal). **Hiroaki Hasebe:** Conceptualization (supporting); Data curation (supporting); Methodology (equal); Supervision (supporting);

Writing – review & editing (supporting). **Hiroshi Sugimoto**: Conceptualization (equal); Investigation (equal); Supervision (equal); Writing – review & editing (equal). **Minoru Fujii**: Funding acquisition (equal); Project administration (equal); Supervision (equal); Writing – review & editing (equal).

DATA AVAILABILITY

The data that support the findings of this study are available from the corresponding authors upon reasonable request.

REFERENCES

- ¹T. J. T. P. van den Berg and H. Spekreijse, *Vis. Res.* **37**, 249 (1997).
- ²H. Kaushal and G. Kaddoum, *IEEE Commun. Surv. Tutor.* **19**, 57 (2017).
- ³M. Casalino, G. Coppola, R. M. de La Rue, and D. F. Logan, *Laser Photonics Rev.* **10**, 895 (2016).
- ⁴M. W. Knight, H. Sobhani, P. Nordlander, and N. J. Halas, *Science* **332**, 702 (2011).
- ⁵C. Clavero, *Nat. Photonics* **8**, 95 (2014).
- ⁶A. Sobhani, M. W. Knight, Y. Wang, B. Zheng, N. S. King, L. V. Brown, Z. Fang, P. Nordlander, and N. J. Halas, *Nat. Commun.* **4**, 1643 (2013).
- ⁷M. Casalino, G. Coppola, M. Iodice, I. Rendina, and L. Sirloto, *Opt. Express* **20**, 12599 (2012).
- ⁸W. Li and J. Valentine, *Nano Lett.* **14**, 3510 (2014).
- ⁹M. Tanzid, A. Ahmadvand, R. Zhang, B. Cerjan, A. Sobhani, S. Yazdi, P. Nordlander, and N. J. Halas, *ACS Photonics* **5**, 3472 (2018).
- ¹⁰H. Y. Fan and A. K. Ramdas, *J. Appl. Phys.* **30**, 1127 (1959).
- ¹¹S. Reiter, N. Koper, R. Reineke-Koch, Y. Larionova, M. Turcu, J. Krügener, D. Tetzlaff, T. Wietler, U. Höhne, J. D. Kähler, R. Brendel, and R. Peibst, *Energy Procedia* **92**, 199 (2016).
- ¹²M. Garin, R. Fenollosa, R. Alcubilla, L. Shi, L. F. Marsal, and F. Meseguer, *Nat. Commun.* **5**, 3440 (2014).
- ¹³W. B. Jackson, N. M. Johnson, and D. K. Biegelsen, *Appl. Phys. Lett.* **43**, 195 (1983).
- ¹⁴H. Hasebe, K. Moriasa, K. Yamashita, H. Sugimoto, and M. Fujii, *ACS Photonics* **9**, 3302 (2022).
- ¹⁵L. Hüttenhofer, A. Tittl, L. Kühner, E. Cortés, and S. A. Maier, *ACS Photonics* **8**, 1469 (2021).
- ¹⁶L. Hüttenhofer, F. Eckmann, A. Lauri, J. Cambiasso, E. Pensa, Y. Li, E. Cortés, I. D. Sharp, and S. A. Maier, *ACS Nano* **14**, 2456 (2020).
- ¹⁷T. Zhang, Y. Che, K. Chen, J. Xu, Y. Xu, T. Wen, G. Lu, X. Liu, B. Wang, X. Xu, Y.-S. Duh, Y.-L. Tang, J. Han, Y. Cao, B.-O. Guan, S.-W. Chu, and X. Li, *Nat. Commun.* **11**, 3027 (2020).
- ¹⁸L. Xu, M. Rahmani, K. Zangeneh Kamali, A. Lamprianidis, L. Ghirardini, J. Sautter, R. Camacho-Morales, H. Chen, M. Parry, I. Staude, G. Zhang, D. Neshev, and A. E. Miroshnichenko, *Light Sci. Appl.* **7**, 44 (2018).
- ¹⁹J. Wang, A. Chen, Y. Zhang, J. Zeng, Y. Zhang, X. Liu, L. Shi, and J. Zi, *Phys. Rev. B* **100**, 075407 (2019).
- ²⁰J. R. Piper, V. Liu, and S. Fan, *Appl. Phys. Lett.* **104**, 251110 (2014).
- ²¹S. Fan, W. Suh, and J. D. Joannopoulos, *J. Opt. Soc. Am. A* **20**, 569 (2003).
- ²²R. Alaei, M. Albooyeh, and C. Rockstuhl, *J. Phys. D: Appl. Phys.* **50**, 503002 (2017).
- ²³R. Xu and J. Takahara, *Opt. Lett.* **46**, 805 (2021).
- ²⁴J. Tian, Q. Li, P. A. Belov, R. K. Sinha, W. Qian, and M. Qiu, *ACS Photonics* **7**, 1436 (2020).
- ²⁵C. Y. Yang, J. H. Yang, Z. Y. Yang, Z. X. Zhou, M. G. Sun, V. E. Babicheva, and K. P. Chen, *ACS Photonics* **5**, 2596 (2018).
- ²⁶C. W. Hsu, B. Zhen, A. D. Stone, J. D. Joannopoulos, and M. Soljačić, *Nat. Rev. Mater.* **1**, 16048 (2016).
- ²⁷K. Koshelev, G. Favraud, A. Bogdanov, Y. Kivshar, and A. Fratallocchi, *Nanophotonics* **8**, 725 (2019).
- ²⁸G. Yang, S. U. Dev, M. S. Allen, J. W. Allen, and H. Harutyunyan, *Nano Lett.* **22**, 2001 (2022).
- ²⁹N. Bernhardt, K. Koshelev, S. J. U. White, K. W. C. Meng, J. E. Fröch, S. Kim, T. T. Tran, D. Y. Choi, Y. Kivshar, and A. S. Solntsev, *Nano Lett.* **20**, 5309 (2020).
- ³⁰L. Carletti, S. S. Kruk, A. A. Bogdanov, C. de Angelis, and Y. Kivshar, *Phys. Rev. Res.* **1**, 023016 (2019).
- ³¹H. Hu, T. Weber, O. Bienek, A. Wester, L. Hüttenhofer, I. D. Sharp, S. A. Maier, A. Tittl, and E. Cortés, *ACS Nano* **16**, 13057 (2022).
- ³²J. Wang, J. Kühne, T. Karamanos, C. Rockstuhl, S. A. Maier, and A. Tittl, *Adv. Funct. Mater.* **31**, 2104652 (2021).
- ³³L. Kühner, L. Sortino, R. Berté, J. Wang, H. Ren, S. A. Maier, Y. Kivshar, and A. Tittl, *Nat. Commun.* **13**, 4992 (2022).
- ³⁴M.-S. Hwang, H.-C. Lee, K.-H. Kim, K.-Y. Jeong, S.-H. Kwon, K. Koshelev, Y. Kivshar, and H.-G. Park, *Nat. Commun.* **12**, 4135 (2021).
- ³⁵M.-S. Hwang, K.-Y. Jeong, J.-P. So, K.-H. Kim, and H.-G. Park, *Commun. Phys.* **5**, 106 (2022).
- ³⁶F. Wu, C. Fan, K. Zhu, J. Wu, X. Qi, Y. Sun, S. Xiao, H. Jiang, and H. Chen, *Phys. Rev. B* **105**, 245417 (2022).
- ³⁷X. Sun, J. Sun, Z. Wang, L. Wang, F. Qiu, and L. Wen, *Nano Lett.* **22**, 9982 (2022).
- ³⁸H. Hasebe, H. Sugimoto, T. Hinamoto, and M. Fujii, *Adv. Opt. Mater.* **8**, 2001148 (2020).
- ³⁹E. A. Gurvitz, K. S. Ladutenko, P. A. Dergachev, A. B. Evlyukhin, A. E. Miroshnichenko, and A. S. Shalin, *Laser Photonics Rev.* **13**, 1800266 (2019).
- ⁴⁰M. Hu, A. Ghoshal, M. Marquez, and P. G. Kik, *J. Phys. Chem. C* **114**, 7509 (2010).
- ⁴¹T. Xu, M. S. Wheeler, H. E. Ruda, M. Mojahedi, and J. S. Aitchison, *Opt. Express* **17**, 8343 (2009).
- ⁴²B. Gallinet and O. J. F. Martin, *ACS Nano* **5**, 8999 (2011).
- ⁴³J. Zhao, C. Zhang, P. V. Braun, and H. Giessen, *Adv. Mater.* **24**, OP247 (2012).
- ⁴⁴W. C. Shih, G. M. Santos, F. Zhao, O. Zenasni, and M. M. P. Arnob, *Nano Lett.* **16**, 4641 (2016).
- ⁴⁵Y. Xu, P. Bai, X. Zhou, Y. Akimov, C. E. Png, L. K. Ang, W. Knoll, and L. Wu, *Adv. Opt. Mater.* **7**, 1801433 (2019).
- ⁴⁶G. Allison, A. K. Sana, Y. Ogawa, H. Kato, K. Ueno, H. Misawa, K. Hayashi, and H. Suzuki, *Nat. Commun.* **12**, 6483 (2021).
- ⁴⁷B. Spackova, P. Wrobel, M. Bockova, and J. Homola, *Proc. IEEE* **104**, 2380 (2016).
- ⁴⁸S. Celiksoy, W. Ye, K. Wandner, K. Kaefer, and C. Sönnichsen, *Nano Lett.* **21**, 2053 (2021).
- ⁴⁹A. Tognazzi, D. Rocco, M. Gandolfi, A. Locatelli, L. Carletti, and C. de Angelis, *Optics* **2**, 193 (2021).